Supporting information

A proof-of-concept electroreduction-free anodic stripping voltammetry analysis of Ag(I) based on S,N-$Ti_3C_2T_x$ MXene nanoribbons

Yifan Zhou,[a,e] Yinhui Yi,[a,b,c] Yong He[c] and Gangbing Zhu*[a,d]

[a] School of Emergency Management, School of the Environment and Safety Engineering, Jiangsu University, Zhenjiang, 212013, P. R. China. E-mail: zhgb1030@ujs.edu.cn

[b] The Key Laboratory of Synthetic and Biological Colloids, Ministry of Education, Jiangnan University, P. R. China

[c] Laboratory of Spectroscopy Sensing, Ministry of Agriculture and Rural Affairs, Zhejiang University, Hangzhou 310058, P.R. China

[d] Key Laboratory of Optic-electric Sensing and Analytical Chemistry for Life Science, MOE, P.R. China

[e] School of Water, Energy and Environment, Cranfield University, Cranfield, Beds, MK430AL, UK

*Corresponding author.
E-mail address: zhgb1030@ujs.edu.cn.

Experimental

Materials and chemicals

KOH, LiF, HCl, Ti_3AlC_2 and $AgNO_3$ were purchased from Sinopharm Chemical Reagent Co., Ltd., whereas L-cysteine (L-cys) was obtained from Shanghai Aladdin Biochemical Technology Co., Ltd. Interfering ion solutions containing metal ions such as Ni^{2+}, Pb^{2+}, Co^{2+}, Mn^{2+}, Zn^{2+} and Cu^{2+} were prepared using the related metal salts as the raw materials. All electrochemical tests were conducted using a CHI 660E electrochemical workstation in a PBS buffer solution (0.1 M, pH 5.0), unless otherwise specified.

Synthesis of S,N-$Ti_3C_2T_xR$

To begin with, $Ti_3C_2T_xS$ was produced through a top-down etching approach to remove the Al layer of Ti_3AlC_2 [1]. Subsequently, $Ti_3C_2T_xR$ was prepared using the following procedure: 250.0 mg of $Ti_3C_2T_xS$ was added into a 30.0 mL solution of 6.0 M KOH, subjected to ultrasonic oscillation for 15 minutes to achieve uniform dispersion, and then stirred continuously for approximately 4 days. After the completion of the reaction, the formed materials were neutralized through washing, subsequently dried at 60°C to obtain black $Ti_3C_2T_xR$ powder.

The final product S,N-$Ti_3C_2T_xR$ was obtained through a straightforward hydrothermal method involving the dissolution of 20.0 mg L-cys in 30.0 mL $Ti_3C_2T_xR$ solution (1.0 mg mL^{-1}). This mixture was then transferred to a Teflon-lined stainless-steel autoclave for the hydrothermal treatment of 12 hours. Afterward, the resulting nanomaterial was subjected to centrifuging, filtering, washing, and drying at 60 °C to acquire the desired S,N-$Ti_3C_2T_xR$ product.

EfASV detection of Ag^+ based on S,N-$Ti_3C_2T_xR$ modified electrode

To prepare the S,N-$Ti_3C_2T_xR$ modified glassy carbon electrode (S,N-$Ti_3C_2T_xR$/GCE), the first step involved carefully polishing the GCE with alumina powder and rinsing it with ultrapure water. Then,

9.0 μL S,N-$Ti_3C_2T_xR$ suspension was added dropwise onto the GCE surface. Then, the modified electrode was subsequently dried using an infrared lamp, resulting in the formation of the desired S,N-$Ti_3C_2T_xR$/GCE. Finally, the EfASV measurement of Ag^+ was conducted in 2-consecutive processes:

(1) Immersing the as-prepared S,N-$Ti_3C_2T_xR$/GCE in a phosphate-buffered saline (PBS) solution containing Ag^+ for a specific duration;

(2) Electrochemical measurements conducted using DPV in a blank 0.1 M PBS solution.

For comparison, $Ti_3C_2T_xS$/GCE and $Ti_3C_2T_xR$/GCE were prepared using identical procedures with above.

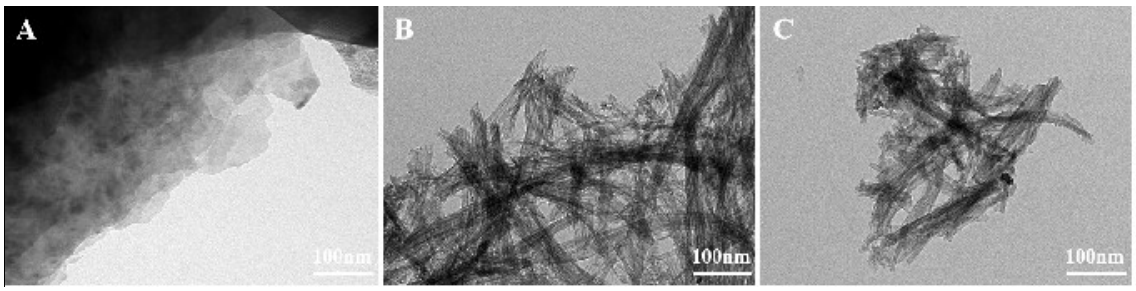

Figure S1. TEM images of $Ti_3C_2T_xS$ (A), $Ti_3C_2T_xR$ (B) and S,N-$Ti_3C_2T_xR$ (C).

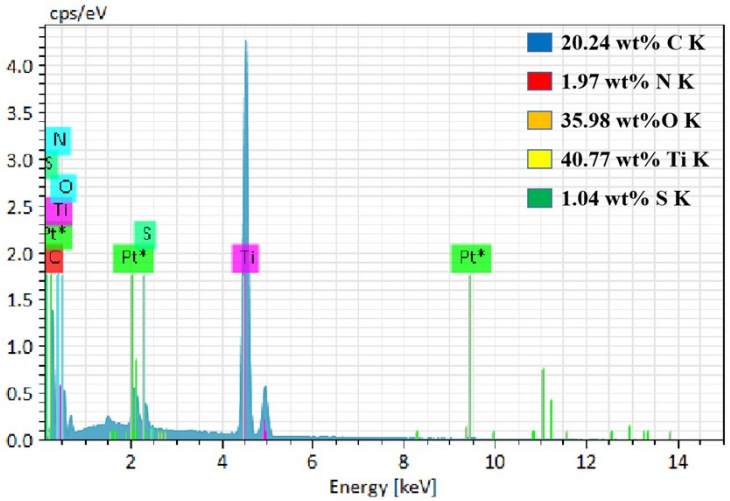

Figure S2. EDS analysis of S, N-$Ti_3C_2T_xR$.

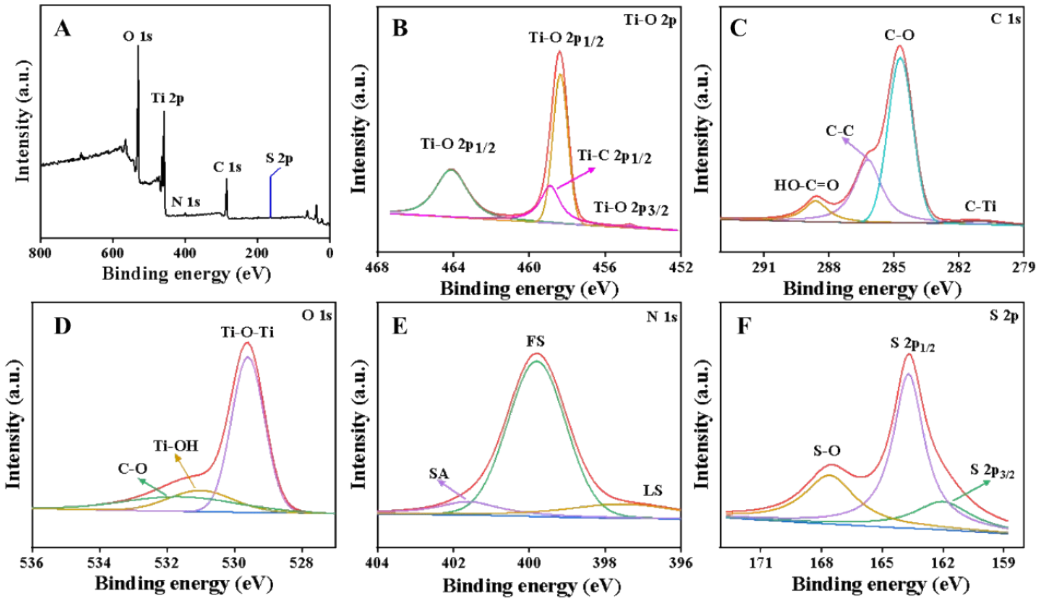

Figure S3. (A) XPS spectra of S,N-$Ti_3C_2T_xR$; high-resolution XPS spectra of (B) Ti 2p spectra, (C) C 1s spectra, (D) O 1s spectra, (E) N 1s spectra, and (F) S 2p spectra of S,N-$Ti_3C_2T_xR$.

It can be found from Figure S3A that the as-prepared S,N- $Ti_3C_2T_xR$ consists of Ti, O, C, N, and S. Figure S3B confirms the presence of a distinct Ti 2p response which can be further resolved into two binding energies, Ti $2p_{1/2}$ and Ti $2p_{3/2}$. The distinct peaks at 288.6 eV, 531.1 eV, and 531.8 eV (Figures S3C and S3D) were attributed to the HO-C=O bond, Ti-OH bond, and CO bond, respectively. The characteristic peaks of N 1s (Figure S3E) and S 2p (Figure S3F) indicate the successful inclusion of N and S heteroatoms, and the spectrogram reveals that the N 1s core energy degree is divided into 3 peaks: the peaks at 401.6 eV, 399.5 eV and 397.3 eV which represent graphite N, pyrolysis N and pyridinic N respectively. In particular, the presence of pyridinic N at 397.2 eV is a crucial factor in improving the electrochemical activity and conductivity [2, 3]. Additionally, the presence of C-SO_x-C (167.6 eV), C-S-C (163.6 eV), and S-Ti (162.0 eV) bonds in Figure 3F verified the effective introduction of sulfur via the existence of S-C bonds.[4, 5]

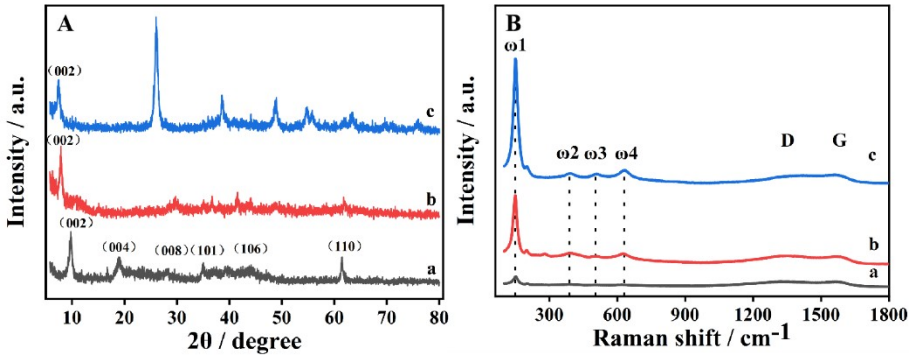

Figure S4. (A) XRD patterns and (B) Raman spectra of (a) $Ti_3C_2T_xS$, (b) $Ti_3C_2T_xR$ and (c) S,N-$Ti_3C_2T_xR$.

The X-ray diffraction (XRD) patterns depicted in Figure S4A provide insights into the structural evolution of the $Ti_3C_2T_xS$, $Ti_3C_2T_xR$, and S,N-$Ti_3C_2T_xR$ powders. The peaks observed at 2θ values of 28.5° and 44.2° correspond respectively to the (008) and (106) planes. After etching, the interlayer spacing of $Ti_3C_2T_xR$ expanded, as evidenced through the shift in the (002) diffraction peak from 2θ=9.7° to 2θ=7.9°, when compared to $Ti_3C_2T_xS$. Additionally, the doping of S and N resulted in a slight shift of the (002) peak to 7.3° in the synthesized S,N-$Ti_3C_2T_xR$, due to the incorporation of heteroelements. This further expanded the interlayer spacing, possibly attributed to the introduction of S, which generated S-O_x at the edges of $Ti_3C_2T_xR$, thereby creating additional accessible active sites and widening the interlayer spacing. The Raman spectrum was employed to evaluate the structure, molecular interactions and defect level in the synthesized $Ti_3C_2T_xS$, $Ti_3C_2T_xR$, and S,N-$Ti_3C_2T_xR$, the results are shown in the Figure S4B. All three spectra exhibit four distinct peaks: the typical peaks at ω1 (~150 cm^{-1}) and ω3 (~508 cm^{-1}) arise from the vibration of TiO_2 anatase phase and Ti atom, while the peaks at ω2 (~385 cm^{-1}) and ω4 (~632 cm^{-1}) represent non-stoichiometric TiC vibrations. Simultaneously, the Raman spectrum also demonstrates the existence of two prominent peaks at ~1345 cm^{-1} and ~1563 cm^{-1}, corresponding to the D band and G band of graphitic C. In general, the D band indicates imperfections in the carbon atom lattice, whereas the G band represents

the sp^2 hybridization of C atom with in-plane stretching vibration. The level of defect structural is commonly quantified by utilizing the intensity ratio of the D and G band (I_D/I_G), and a larger I_D/I_G ratio usually signifies a greater extent of defects. From the figure, the computational findings demonstrate a progressive increase in I_D/I_G values for $Ti_3C_2T_xS$, $Ti_3C_2T_xR$, and S,N-$Ti_3C_2T_xR$, with values of 0.891, 0.970, and 0.985 respectively. This indicates a decline in the graphitization level of the material and an enhancement in defect density, confirming the successful synthesis of S,N-$Ti_3C_2T_xR$ with increased vacancies, defects, and more active sites.

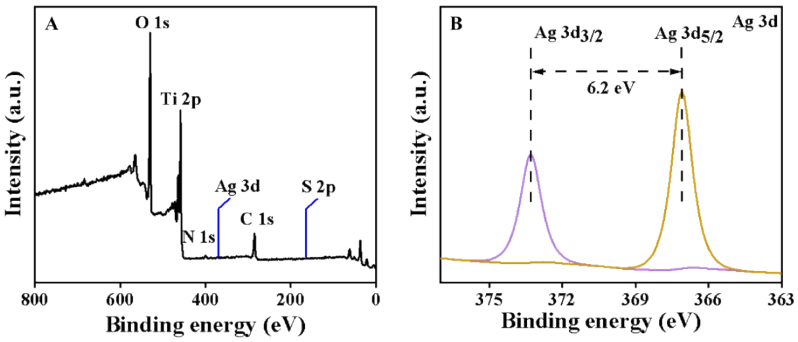

Figure S5. (A) XPS spectra of Ag^0/S,N-$Ti_3C_2T_xR$ and (B) high-resolution XPS spectra of Ag 3d spectra.

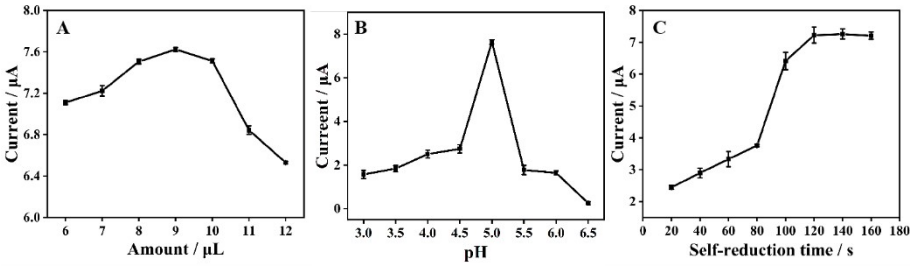

Figure S6. The effect of the pH value of PBS (A), the amount of S,N-$Ti_3C_2T_xR$/GCE (B) and the accumulation time (C) on the DPV peak currents of Ag^+ (2.0 μM).

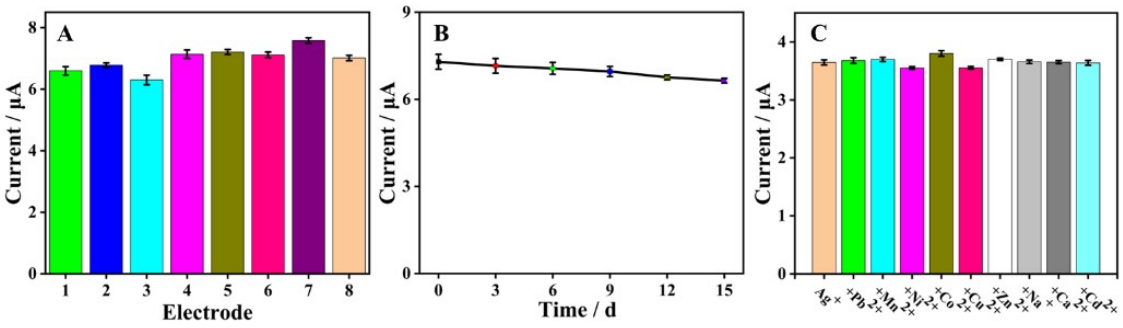

Figure S7. (A) The peak current values of 8 independently fabricated S,N-$Ti_3C_2T_x$R/GCE towards Ag^+ (2.0 μM), (B) the stability test of S,N-$Ti_3C_2T_x$R/GCE/GCE for Ag^+ (2.0 μM) and (C) the peak current values of S,N-$Ti_3C_2T_x$R/GCE/GCE towards Ag^+ (0.2 μM) containing various ions (2.0 μM).

Initially, a total of eight separate S,N-$Ti_3C_2T_x$R/GCEs was prepared by using similar method, and the DPV signal of Ag^+ was subsequently measured simultaneously in 0.1 M PBS. The findings in Figure S7A demonstrated a relative standard deviation (RSD) of 3.72% for the DPV current, indicating the favorable reproducibility of the S,N-$Ti_3C_2T_x$R/GCE. Subsequently, we assessed the sensor stability by storing S,N-$Ti_3C_2T_x$R/GCE at 4 °C for two weeks (Figure S7B). The findings confirmed that the peak current response for Ag^+ remained at 91.1% of its initial value, indicating the outstanding stability of the sensor. Moreover, the selectivity of S,N-$Ti_3C_2T_x$R/GCE was examined by introducing various interfering substances in the test samples. The result display that the presence of ions including Pb^{2+}, Mn^{2+}, Ni^{2+}, Co^{2+}, Cu^{2+}, Zn^{2+}, Na^+, Ca^{2+}, and Cd^{2+} (2.0 μM) did not affect the results when using S,N-$Ti_3C_2T_x$R/GCE to detect Ag^+ (0.2 μM), indicating its strong capability to resist interference, as displayed in Figure S7C.

Table S1. Comparisons between the present EfASV sensor and previously reported ASV sensors for Ag^+ detection.

Sensors	Electrodeposition	Linear range / μM	LOD / nM	Ref
Au@4-ATP/Au	-0.54V, 350s	0.005–3.0	13	6
PANI/SSA/GCE	-0.45V, 100s	0.01-100	3.4	7
Cr/CPE	-1.3V, 100s	0.028-0.093	9.3	8
GaN micropillar electrode	-0.1V, 180s	0.093-9.3	30	9
LB/PAn-PTSA/GCE	-0.56V, 200s	0.006-1.0	0.4	10
MWCNTs/CPE	-0.7V, 20s	0.0046-2.2	0.74	11
Schiff/CPE	-0.7V, 20s	0.0046-1.8	0.85	12
4-tert-butyl-1thiacalix [4] arene	-0.6V, 30s	0.05-30.0	10	13
mag-IIP-NPs/CPE	-0.8V, 40s	0.0046-1.4	1.4	14
CNTs/GCE	0.3V, 240s	0.1-2.5	30	15
BiEF/GCE	-0,8V, 60s	0.093-0.83	19	16
ABP/GA/4-NBD/GCE	-0.6V, 180s	0.05-1.0	25	17
BHAB-MCPE/CPE	-0.9V, 300s	0.01-2.0	6.7	18
N-CNT/GO_x		0.02-0.2	1.8	19
p-isopropylcalix[6]arene/CPE	-0.25V, 180s	0.05-2.0	48	20
S,N-$Ti_3C_2T_xR$/GCE	Free	0.002-4.0	0.667	This work

Table S2. The determination of Ag^+ in real samples.

Sample	Spiked / μM	Found / μM	Recovery / %	RSD / %
Lake water	0.02	0.021	105.0	3.23
	0.2	0.218	109.0	3.42
	2.0	1.980	99.0	5.14
Tap water	0.02	0.019	95.0	4.57
	0.2	0.197	98.5	4.11
	2.0	2.13	106.5	4.05

References

1 J. Liu, X. Jiang, R. Zhang, Y. Zhang, L. Wu, W. Lu, J. Li, Y. Li and H. Zhang, *Advanced Functional Materials*, 2019, **29**, 1807326.

2 Q. Guan, J. Ma, W. Yang, R. Zhang, X. Zhang, X. Dong, Y. Fan, L. Cai, Y. Cao and Y. Zhang, *Nanoscale*, 2019, **11**, 14123-14133.

3 C. Lu, L. Yang, B. Yan, L. Sun, P. Zhang, W. Zhang and Z. Sun, *Advanced Functional Materials*, 2020, **30**, 2000852.

4 W. Zhu, J. Gao, H. Song, X. Lin and S. Zhang, *ACS applied materials interfaces*, 2019, **11**, 44545-44555.

5 Z. Guo, P. Ren, J. Wang, X. Hou, J. Tang, Z. Liu, Z. Chen, Y. Jin and F. Ren, *Chemical Engineering Journal*, 2023, **451**, 138667.

6 Z. Xiao, H. Meng, X. Qin, X. Sang, Y. Zhang and Y. Yuan, *Analyst*, 2021, **146**, 597-604.

7 F. Hashemi and A. R. Zanganeh, *Journal of Electroanalytical Chemistry*, 2016, **767**, 24-33.

8 Z. Koudelkova, T. Syrovy, P. Ambrozova, Z. Moravec, L. Kubac, D. Hynek, L. Richtera and V. Adam, *Sensors*, 2017, **17**, 1832.

9 Q. Liu, J. Li, W. Yang, X. Zhang, C. Zhang, C. Labbé, X. Portier, F. Liu, J. Yao and B. Liu, *Analytica chimica acta*, 2020, **1100**, 22-30.

10 Q. Liu, F. Wang, Y. Qiao, S. Zhang and B. Ye, *Electrochimica acta*, 2010, **55**, 1795-1800.

11 S. Jahandari, M. A. Taher, H. Fazelirad and I. Sheikhshoai, *Microchimica Acta*, 2013, **180**, 347-354.

12 H. H. Nadiki, M. A. Taher, H. Ashkenani and I. Sheikhshoai, *Analyst*, 2012, **137**, 2431-2436.

13 F. Wang, C. Xin, Y. Wu, Y. Gao and B. Ye, *Journal of Analytical Chemistry*, 2011, **66**, 60-65.

14 M. Ghanei-Motlagh and M. A. Taher, *Microchimica Acta*, 2017, **184**, 1691-1699.

15 X. Liu, W. Li, Q. Shen, Z. Nie, M. Guo, Y. Han, W. Liu and S. Yao, *Talanta*, 2011, **85**, 1603-1608.

16 T. Romih, S. B. Hočevar, A. Jemec and D. Drobne, *Electrochimica Acta*, 2016, **188**, 393-397.

17 M.-C. Radulescu, A. Chira, M. Radulescu, B. Bucur, M. P. Bucur and G. L. Radu, *Sensors*, 2010, **10**, 11340-11351.

18 M. Gholivand and M. Parvin, *Electroanalysis*, 2010, **22**, 2291-2296.

19 I. M. Rust, J. M. Goran and K. J. Stevenson, *Analytical chemistry*, 2015, **87**, 7250-7257.

20 J. B. Raoof, R. Ojani, A. Alinezhad and S. Z. Rezaie, *Monatshefte für Chemie-Chemical Monthly*, 2010, **141**, 279-284.